ChemComm

COMMUNICATION

View Article Online
View Journal | View Issue

Cite this: *Chem. Commun.*, 2019, **55**, 1647

Received 20th December 2018,
Accepted 11th January 2019

DOI: 10.1039/c8cc10060h

rsc.li/chemcomm

Polymer grafted on carbon nanotubes as a flexible cathode for aqueous zinc ion batteries†

Xiujun Yue, Haodong Liu and Ping Liu *

We have developed a free-standing, flexible cathode for an aqueous zinc ion battery by grafting cross-linked polydopamine on carbon nanotubes. The cathode is highly stable, with little capacity degradation for 500 cycles. The flexible cathode is environmentally benign and biocompatible which can enable applications from biomedical devices to grid storage.

Driven by the ever increasing demand of environmentally benign, low-cost electrical energy storage solutions, Zn based aqueous batteries are being extensively investigated due to potential advantages in cost, safety, abundancy, and environmental friendliness.[1–4] With a very negative electrical potential of −0.76 V *vs.* SHE, zinc based batteries also offer highly competitive energy densities.[5,6]

Finding a reversible cathode with high capacity has been a major challenge. Intercalation reaction based materials, including oxides of manganese and vanadium, are the current focus.[7–12] Due to the large changes in crystal volume, structure, and morphology during zinc insertion and removal, cycling stability of these materials is usually a concern.[3,13,14] In addition, manganese oxides also suffer severe capacity fading due to Mn^{2+} dissolution associated with the Jahn–Teller effect.[1,15,16] Adding manganese or other salts into the electrolyte is required to alleviate such effects.[17,18] Framework type (*e.g.*, Prussian blue analogs) materials have also been investigated, which offer enhanced cycling stability at the expense of volumetric energy density.[19,20]

Very recently, several attempts have been made to develop organic cathode materials utilizing an energy storage mechanism other than intercalation/deintercalation. For instance, quinone exhibits ion storage capability by coordinating with the metal ions with its oxygen atoms when the carbonyl groups are reduced at low potentials.[21–25] Both high capacity and cycling stability has been achieved by calix[4]quinone (C4Q) when used in a zinc ion battery.[26] Moreover, polymers are expected to have minimal dissolution in the electrolyte and long cycle life due to the stable, covalently connected structure.[27]

Herein, we demonstrate the application of polydopamine (PDA)/carbon nanotube (CNT) composite as a cathode material for aqueous zinc ion batteries (Fig. 1). Inspired by the adhesive protein Mefp5 in mussels, PDA can be coated on a wide range of material surfaces through the spontaneous self-polymerization of dopamine in basic aqueous solution.[28,29]

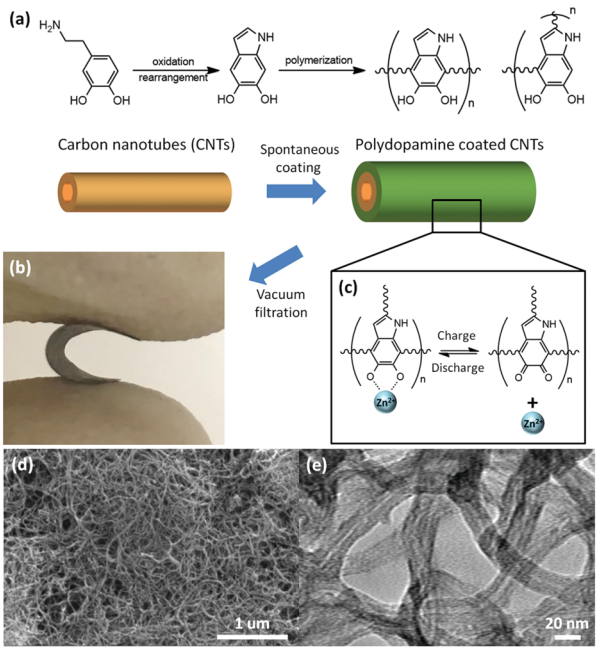

Fig. 1 (a) Fabrication of PDA electrode by the spontaneous self-polymerization of dopamine on CNT supporting in basic aqueous solution. (b) Photo of a flexible free-standing CNT supported PDA thin film electrode. (c) Schematic of zinc ion adsorption by catechol and desorption by *ortho*-quinone when PDA at discharged or charged states, respectively. (d) Scanning electron microscopy (SEM). (e) Transmission electron microscopy (TEM) images of PDA electrode.

Department of Nanoengineering, University of California San Diego, La Jolla, CA 92093, USA. E-mail: piliu@eng.ucsd.edu

† Electronic supplementary information (ESI) available. See DOI: 10.1039/c8cc10060h

In each building unit, two redox-active quinone groups are available for zinc ion storage *via* the reversible catechol/*ortho*-quinone reaction (Fig. 1(c)).[30–32] Compared to other organic cathodes for zinc-ion batteries, PDA has several advantages: (1) PDA has low solubility in water which mitigates capacity loss during cycling. Additionally, the hydrophilic nature of PDA ensures excellent wetting at the electrode/electrolyte interface, whereas many other polymer cathodes are hydrophobic;[33] (2) due to the bio-adhesion effect, PDA enhance the structural stability of composite electrode as it adheres to the conductive CNT strongly which results in high rate capability. In comparison, polymer cathodes are usually physically mixed with large amount of carbon, making it difficult to achieve a highly efficient conductive network; (3) with a similar structure and function to natural eumelanins, PDA exhibits high biocompatibility and low cytotoxicity.[34] Indeed, a Zn/PDA battery with an aqueous electrolyte at a neutral pH would be substantially non-hazardous and highly desirable for biomedical devices; and (4) the PDA/CNT electrode is highly flexible which makes it possible to fabricate conformal batteries, also essential for biomedical applications.

We developed a flexible, free-standing, binder-free cathode for rechargeable aqueous zinc ion battery based on CNT supported PDA (Fig. 1(a and b)). PDA was coated on dispersed CNT by spontaneous polymerization of dopamine in a basic aqueous solution. Followed by vacuum-filtering the mixture dispersion, the free-standing thin film electrode was assembled while removing unreacted monomers. Outstanding flexibility of the thin film electrode is achieved due to the bio-adhesion nature of PDA (Video in ESI†). SEM images show the PDA coated CNTs in the electrode were well-dispersed but also well-connected (Fig. 1(d)). TEM images show that the PDA was uniformly coated onto CNT with a thickness of 8 nm (Fig. 1(e)). No aggregated PDA nanoparticles were found in either TEM or SEM images.

Cyclic voltammetry (CV) was first performed to assess the electrochemical behaviour of PDA as cathode material for zinc ion batteries (Fig. 2(a)). The PDA electrode was assembled into a coin cell with zinc foil as the anode, a filter paper as separator, and 3.3 M $ZnSO_4$ aqueous solution as the electrolyte. CV curves were obtained by scanning between 0.3 and 1.4 V *vs.* Zn^{2+}/Zn at a rate of 1 mV s^{-1}. The scanning begins with reduction (zinc ion adsorption) since the pristine PDA electrode contains no zinc ion. In both initial anodic and cathodic scans, strong but not well-defined features were observed (Fig. S2, ESI†). After about 20 cycles, the peak current decreases and the curve gradually develops into a pair of wide and well-defined reduction/oxidation peaks at 0.91/1.15 V. Those two peaks correspond to the reversible reaction between catechol and *ortho*-quinone along with zinc ion adsorption/desorption. The CV curve shape change and capacity drop during initial cycles are likely related to the non-covalently bonded dopamine monomer and intermediate species assembled in the PDA structure, which will be discussed further later. The linear relationship between the peak current and scan rate indicated the redox reaction of PDA is controlled by a surface process (Fig. 2(b)), similar to the mechanism operating in pseudo-capacitors.

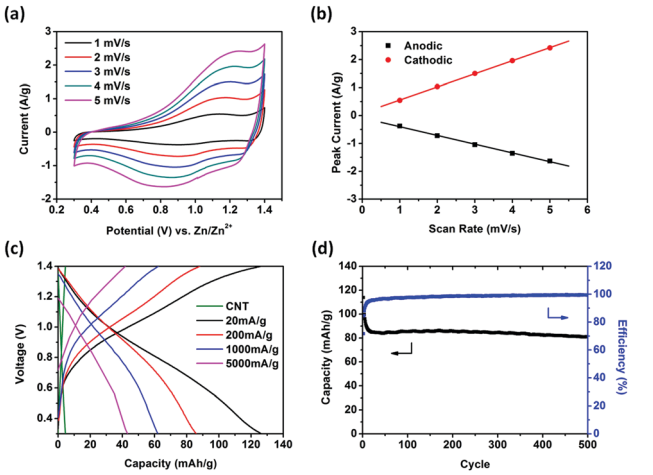

Fig. 2 Electrochemical performances of PDA electrodes. (a) Cyclic voltammetry (CV) profiles at different scan rate. (b) CV peak current as a function of scan rate (c). Galvanostatic charge/discharge curves of PDA electrodes at different current densities and blank CNT thin film electrode at 200 mA g^{-1}. 20 mA g^{-1} curves was from 30th cycle. All other data were from 100th cycle. (d) Long term cyclic performance at 200 mA g^{-1} for 500 cycles. All tests were in coin cells at the potential range of 0.3–1.4 V, with zinc metal foil as anode and 3.3 M $ZnSO_4$ aqueous solution as electrolyte.

The cycling stability of PDA was evaluated by galvanostatic charge and discharge at a potential range of 0.3–1.4 V *vs.* Zn^{2+}/Zn. As shown in the Fig. 2(c), the PDA electrode delivered a capacity of 126.2 mA h g^{-1} at a low rate of 20 mA g^{-1}. The electrode is capable of exceptionally high rates, delivering 43.2 mA h g^{-1} at 5000 mA g^{-1}. Note that the majority of the loss is related to an IR drop which can be further improved by cell design. The high rate performance is consistent with the capacitive mechanism observed in CV studies. The capacity of CNT itself was also examined by fabricating free standing CNT thin film electrode with the same vacuum-filtration method. When discharged at 200 mA g^{-1}, the CNT thin film electrode can only deliver a capacity of 4.5 mA h g^{-1}, thus contributing very little to the CNT supported PDA electrode. The volumetric capacity of PDA electrode is moderate as shown in Fig. S4 (ESI†). However, this does not preclude the application in biomedical devices and grid storage since unique advantages in flexibility, environmental friendliness, and cycle life are our main concern. The cycling performance of PDA was evaluated at a constant current density of 200 mA g^{-1} (Fig. 2(d)). After about 20 cycles, the battery reached a steady state and delivered a stable capacity of PDA for over 500 cycles. The 500th cycle maintained 96% capacity of the 20th cycle, which is attributed to the stable covalent cross-linked PDA structure and the highly reversible redox reaction of catechol/*ortho*-quinone groups. The high coulombic efficiency of about 99.4% also supports the outstanding reversibility of the redox reaction.

The energy storage mechanism of PDA as a cathode material for zinc ion batteries was investigated by a comparison of *ex situ* Fourier-transform infrared (FT-IR) before and after electrochemical oxidation (Fig. 3(a)). The complex spectra in the

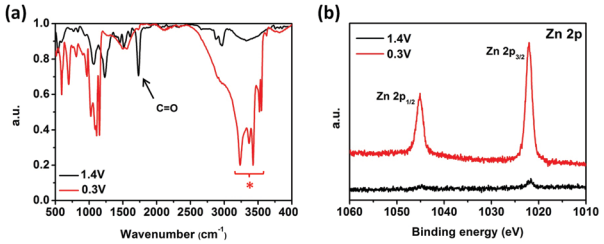

Fig. 3 *Ex situ* spectroscopic analysis of PDA electrodes at charged (1.4 V) and discharged (0.3 V) states. (a) FT-IR. (b) High resolution XPS Zn 2p. All electrodes were cycled between 0.3–1.4 V in 3.3 M $ZnSO_4$ aqueous electrolyte for 20 cycles at 200 mA g^{-1}, then charged or discharged to noted potentials. Peaks noted with the asterisk symbol represent N–H, O–Zn–O structure, and possible intermolecular bonds.

3300 to 3600 cm^{-1} region on the sample reduced at 0.3 V correspond to N–H, O–Zn–O and possible intermolecular bonds, which virtually disappeared when the electrode was charged (oxidized) to 1.4 V. In addition, a C═O bond signal at 1730 cm^{-1} appeared after charging, which supports the formation of a quinone structure. The double-peak at 2870, 2960 cm^{-1} and signals below 1600 cm^{-1} belong to the features of the indole structure, which exist all the time. The changes of FT-IR spectra clearly prove the reversible redox reaction between catechol and *ortho*-quinone of PDA.

Ex situ X-ray photoelectron spectroscopy (XPS) tests were performed to further analyze the energy storage mechanism of PDA. The wide-range XPS spectra for charged and discharged PDA electrodes exhibit almost identical signals for H, C, N and O (Fig. S5, ESI†). However, after repeated rinsing with water, only the spectra of discharged PDA electrode clearly shows a series of zinc features, including 2p, 3s, 3p, 3d and several auger LMM peaks, indicative of significant amounts of zinc ions binding to the catechols. The difference is more evident in the high resolution Zn 2p spectra (Fig. 3(b)). The charged PDA electrode exhibits negligible signal from Zn $2p_{1/2}$. The signal from Zn $2p_{3/2}$ is less than 5% of the peak area of discharged PDA, which might be due to residual $ZnSO_4$ electrolyte. It is well known that catechols have a strong binding affinity to multivalent cations and such interaction is significantly suppressed when oxidized to *ortho*-quinones.[35] Our observation is consistent with such a mechanism involving the reversible reaction between PDA and zinc ions.

We note that there is a capacity loss process during the first twenty cycles before stabilizing for hundreds of cycles. High resolution XPS was utilized to understand this phenomenon *via* examining the structure of PDA electrode. As-prepared pristine PDA electrode was first studied (Fig. S6, ESI†). The C 1s spectra can be deconvoluted into four peaks: CH_x, C–NH_2 and sp^2-hybridized carbon at 284.20 eV, C–O and C–N at 285.25 eV, C═O at 287.75 eV, and $\pi \rightarrow \pi^*$ for aromatic carbon species at 290.95 eV. The result matches with reported PDA materials.[36] The O 1s signals at 531.45 and 532.85 eV correspond to C═O and C–O in the quinone/catechol structure, respectively, indicating the PDA electrode is a mixture of quinone and catechol in its as-synthesized form. The N 1s spectrum can be deconvoluted into one dominating peak at 399.70 eV corresponding to secondary amine (R_2NH), while the peaks at 401.45 eV and 398.45 eV can be assigned to primary amine (RNH_2) and tertiary or aromatic amine groups (═N-R), respectively. The presence of three different peaks indicated that the pristine PDA electrode contains not only PDA but also dopamine monomers and some intermediate species, consistent with the formation mechanism of PDA proposed by several recent studies (Fig. S1, ESI†).[37–40] The primary amine peak, 21% of the total N 1s signal, is indicative of unreacted dopamine monomers even after an extended polymerization reaction time. The tertiary amine intermediate specie contributes to about 7% of the total. The secondary amine peak, contributing 72% to the N 1s signal, is associated with both PDA and intermediate species. This is because the tertiary amine intermediate specie is a tautomer of secondary amine intermediate species. The presence of one type of intermediate specie indicates the co-existence of the other. We hypothesize that the non-negligible amount of non-covalently assembled dopamine and intermediate species in the pristine PDA electrodes are responsible for the initial capacity loss due to their dissolution in the electrolyte in ionized forms.

To further confirm our hypothesis, *ex situ* XPS was performed. In the N 1s XPS spectrum of PDA electrode which has been cycled and reached steady-state capacity (Fig. 4), the ratio of the primary amine peak, belonging to unreacted dopamine, decreases from 21% to 5% when compared with the pristine electrode. This indicates a loss of the primary amine during initial cycling. In the addition, no tertiary amine intermediate specie is observed in the cycled sample means the secondary amine peak is from only PDA. The total amount of non-covalent bonded species decreased from more than 28% to 5% during the process of PDA electrode reaching steady state.

The presence of dopamine monomer in the PDA electrode prior to cycling was also confirmed *via* UV-vis spectroscopy (Fig. S7, ESI†). Since CNT has strong signals in the UV range, PDA nanoparticles were prepared for these tests. Even after repeated washing, a strong peak at 280 nm, attributable to the dopamine monomer, can still be observed in PDA particles. The peak at 320 nm can be assigned to intermediate species. Hence, during the initial cycles, non-covalently bonded species provided the extra capacity, which was gradually lost due to their solubility in the electrolyte. This hypothesis was further examined by a pre-cycling process. The pristine PDA electrode was pre-cycled for 50 cycles at 200 mA g^{-1} first. The electrode

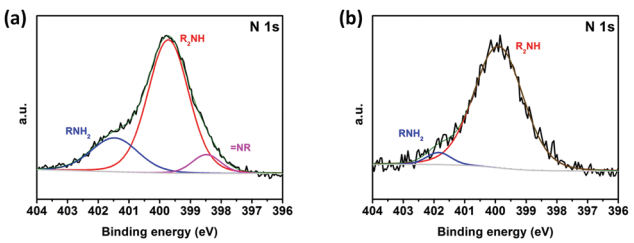

Fig. 4 *Ex situ* high resolution XPS N 1s spectrums of PDA electrodes. (a) Before cycling. (b) After cycling.

was then washed, dried, and re-assembled into a new battery. As shown in Fig. S8 (ESI†), when cycled at 200 mA g^{-1}, the pre-cycled PDA electrode exhibited less significant initial capacity decay as compared with the pristine one. The stable capacity was increased from 86.0 mA h g^{-1} to 92.9 mA h g^{-1}, while many fewer cycles were needed for the capacity to stabilize. It is thus important to remove the encapsulated monomers as much as possible to obtain highly stable polymer cathodes.

In conclusion, we have demonstrated polydopamine (PDA) as a new organic cathode material for aqueous zinc ion battery. A flexible, free-standing, binder-free PDA cathode was fabricated with CNT as support. The PDA delivers a low-rate specific capacity of 126.2 mA h g^{-1}. After an initial stabilization period, outstanding long term stability was observed: after 500 cycles, the PDA electrode still retained 96% of the stabilized capacity. CV studies indicate the electrode reaction is a surface process, similar to that in electrochemical capacitors. FT-IR and XPS studies have established the reaction mechanism to be the redox reaction between catechol and *ortho*-quinone accompanied by zinc ion adsorption and desorption. The non-toxic, flexible PDA has great potential to broaden the application of aqueous zinc ion battery, including in biomedical devices.

We thank the University of California, San Diego for financial support. This work was performed in part at the San Diego Nanotechnology Infrastructure (SDNI) of UCSD, a member of the National Nanotechnology Coordinated Infrastructure, which is supported by the National Science Foundation (Grant ECCS-1542148). Part of the work used the UCSD-MTI Battery Fabrication Facility and the UCSD-Arbin Battery Testing Facility. The authors would like to thank Dr Ich Tran for his help with the XPS experiments at the University of California, Irvine Materials Research Institute (IMRI) using instrumentation funded in part by the National Science Foundation Major Research Instrumentation Program under Grant No. CHE-1338173.

Conflicts of interest

There are no conflicts to declare.

Notes and references

1 M. Song, H. Tan, D. Chao and H. J. Fan, *Adv. Funct. Mater.*, 2018, **28**, 1802564.
2 X. G. Zhang, *Corrosion and Electrochemistry of Zinc*, Springer US, New York, 1996.
3 C. Xu, B. Li, H. Du and F. Kang, *Angew. Chem., Int. Ed.*, 2012, **51**, 933–935.
4 J. Muldoon, C. B. Bucur and T. Gregory, *Chem. Rev.*, 2014, **114**, 11683–11720.
5 L. Zhang, L. Chen, X. Zhou and Z. Liu, *Adv. Energy Mater.*, 2015, **5**, 1400930.
6 A. Konarov, N. Voronina, J. H. Jo, Z. Bakenov, Y.-K. Sun and S.-T. Myung, *ACS Energy Lett.*, 2018, **3**, 2620–2640.
7 D. Kundu, B. D. Adams, V. Duffort, S. H. Vajargah and L. F. Nazar, *Nat. Energy*, 2016, **1**, 16119.
8 F. Wang, O. Borodin, T. Gao, X. Fan, W. Sun, F. Han, A. Faraone, J. A. Dura, K. Xu and C. Wang, *Nat. Mater.*, 2018, **17**, 543–549.
9 X. Wu, Y. Xiang, Q. Peng, X. Wu, Y. Li, F. Tang, R. Song, Z. Liu, Z. He and X. Wu, *J. Mater. Chem. A*, 2017, **5**, 17990–17997.
10 N. Zhang, F. Cheng, Y. Liu, Q. Zhao, K. Lei, C. Chen, X. Liu and J. Chen, *J. Am. Chem. Soc.*, 2016, **138**, 12894–12901.
11 P. He, Y. Quan, X. Xu, M. Yan, W. Yang, Q. An, L. He and L. Mai, *Small*, 2017, **13**, 1702551.
12 B. Sambandam, V. Soundharrajan, S. Kim, M. H. Alfaruqi, J. Jo, S. Kim, V. Mathew, Y.-k. Sun and J. Kim, *J. Mater. Chem. A*, 2018, **6**, 3850–3856.
13 M. H. Alfaruqi, V. Mathew, J. Gim, S. Kim, J. Song, J. P. Baboo, S. H. Choi and J. Kim, *Chem. Mater.*, 2015, **27**, 3609–3620.
14 E. Chae, J. Gim, J. Song, S. Kim, V. Mathew, J. Han, S. Boo and J. Kim, *RSC Adv.*, 2013, **3**, 26328–26333.
15 J. Ming, J. Guo, C. Xia, W. Wang and H. N. Alshareef, *Mater. Sci. Eng., R*, 2019, **135**, 58–84.
16 B. Lee, H. R. Seo, H. R. Lee, C. S. Yoon, J. H. Kim, K. Y. Chung, B. W. Cho and S. H. Oh, *ChemSusChem*, 2016, **9**, 2948–2956.
17 N. Zhang, F. Cheng, J. Liu, L. Wang, X. Long, X. Liu, F. Li and J. Chen, *Nat. Commun.*, 2017, **8**, 405.
18 H. Pan, Y. Shao, P. Yan, Y. Cheng, K. S. Han, Z. Nie, C. Wang, J. Yang, X. Li, P. Bhattacharya, K. T. Mueller and J. Liu, *Nat. Energy*, 2016, **1**, 16039.
19 Z. Jia, B. Wang and Y. Wang, *Mater. Chem. Phys.*, 2015, **149–150**, 601–606.
20 Z. Liu, P. Bertram and F. Endres, *J. Solid State Electrochem.*, 2017, **21**, 2021–2027.
21 T. Liu, K. C. Kim, B. Lee, Z. Chen, S. Noda, S. S. Jang and S. W. Lee, *Energy Environ. Sci.*, 2017, **10**, 205–215.
22 Y. Liang, Y. Jing, S. Gheytani, K.-Y. Lee, P. Liu, A. Facchetti and Y. Yao, *Nat. Mater.*, 2017, **16**, 841.
23 G. Milczarek and O. Inganäs, *Science*, 2012, **335**, 1468–1471.
24 Y. Liang, Z. Tao and J. Chen, *Adv. Energy Mater.*, 2012, **2**, 742–769.
25 B. Pan, D. Zhou, J. Huang, L. Zhang, A. K. Burrell, J. T. Vaughey, Z. Zhang and C. Liao, *J. Electrochem. Soc.*, 2016, **163**, A580–A583.
26 Q. Zhao, W. Huang, Z. Luo, L. Liu, Y. Lu, Y. Li, L. Li, J. Hu, H. Ma and J. Chen, *Sci. Adv.*, 2018, **4**, eaao1761.
27 G. Dawut, Y. Lu, L. Miao and J. Chen, *Inorg. Chem. Front.*, 2018, **5**, 1391–1396.
28 H. Lee, S. M. Dellatore, W. M. Miller and P. B. Messersmith, *Science*, 2007, **318**, 426–430.
29 M. Xiao, Y. Li, M. C. Allen, D. D. Deheyn, X. Yue, J. Zhao, N. C. Gianneschi, M. D. Shawkey and A. Dhinojwala, *ACS Nano*, 2015, **9**, 5454–5460.
30 M. d'Ischia, A. Napolitano, A. Pezzella, P. Meredith and T. Sarna, *Angew. Chem., Int. Ed.*, 2009, **48**, 3914–3921.
31 B. Szpoganicz, S. Gidanian, P. Kong and P. Farmer, *J. Inorg. Biochem.*, 2002, **89**, 45–53.
32 Y. J. Kim, W. Wu, S.-E. Chun, J. F. Whitacre and C. J. Bettinger, *Adv. Mater.*, 2014, **26**, 6572–6579.
33 T. H. Yoon and Y. J. Park, *RSC Adv.*, 2014, **4**, 17434–17442.
34 Y. Huang, Y. Li, Z. Hu, X. Yue, M. T. Proetto, Y. Jones and N. C. Gianneschi, *ACS Cent. Sci.*, 2017, **3**, 564–569.
35 H. Lee, N. F. Scherer and P. B. Messersmith, *Proc. Natl. Acad. Sci. U. S. A.*, 2006, **103**, 12999–13003.
36 R. A. Zangmeister, T. A. Morris and M. J. Tarlov, *Langmuir*, 2013, **29**, 8619–8628.
37 Y. Li, M. Liu, C. Xiang, Q. Xie and S. Yao, *Thin Solid Films*, 2006, **497**, 270–278.
38 F. Bernsmann, V. Ball, F. Addiego, A. Ponche, M. Michel, J. J. d. A. Gracio, V. Toniazzo and D. Ruch, *Langmuir*, 2011, **27**, 2819–2825.
39 M. Arzillo, G. Mangiapia, A. Pezzella, R. K. Heenan, A. Radulescu, L. Paduano and M. d'Ischia, *Biomacromolecules*, 2012, **13**, 2379–2390.
40 J. Jiang, L. Zhu, L. Zhu, B. Zhu and Y. Xu, *Langmuir*, 2011, **27**, 14180–14187.

